NACA RM L55E25b

RESEARCH MEMORANDUM

EFFECT OF AUTOMATIC STABILIZATION ON THE SIDESLIP AND ANGLE-OF-ATTACK DISTURBANCES IN ROLLING MANEUVERS

By Ordway B. Gates, Jr., Joseph Weil,
and C. H. Woodling

Langley Aeronautical Laboratory
Langley Field, Va.

NATIONAL ADVISORY COMMITTEE
FOR AERONAUTICS

WASHINGTON

July 15, 1955
Declassified July 17, 1958

NATIONAL ADVISORY COMMITTEE FOR AERONAUTICS

RESEARCH MEMORANDUM

EFFECT OF AUTOMATIC STABILIZATION ON THE SIDESLIP AND ANGLE-OF-ATTACK DISTURBANCES IN ROLLING MANEUVERS

By Ordway B. Gates, Jr., Joseph Weil,
and C. H. Woodling

SUMMARY

Time histories are presented that illustrate the large motions which have been encountered in flight tests of some of the present-day fighter airplanes.

Results of some analog studies are discussed which indicate that variations in certain of the airplane stability derivatives could have an appreciable effect on these undesirable motions.

SYMBOLS

W	weight, lb
m	mass, slugs
I_X	moment of inertia about X body axis, slug-ft^2
I_Y	moment of inertia about Y body axis, slug-ft^2
I_Z	moment of inertia about Z body axis, slug-ft^2
I_{XZ}	product of inertia in XZ-plane, slug-ft^2
I_{X_e}	moment of inertia of engine about X body axis, slug-ft^2
ω_e	rotational velocity of engine, radians/sec

S	wing area, sq ft
b	wing span, ft
c	chord, ft
$\bar{c}$	mean aerodynamic chord, ft
q	dynamic pressure, lb/sq ft
M	Mach number
H_p	pressure altitude, ft
Λ	sweep angle, deg
A	aspect ratio, b^2/S
δ_{a_T}	total aileron deflection, deg
i_t	stabilizer deflection, deg
δ_r	rudder deflection, deg
F_X	aerodynamic forces along X body axis, lb
F_Y	aerodynamic forces along Y body axis, lb
F_Z	aerodynamic forces along Z body axis, lb
l_3,m_3,n_3	direction cosines
L'	aerodynamic rolling moments, lb-ft
M'	aerodynamic pitching moments, lb-ft
N'	aerodynamic yawing moments, lb-ft
u,v,w	linear velocities along X, Y, and Z body axes, ft/sec
p,q,r	angular velocities about X, Y, and Z body axes, radians/sec
$\Delta u,\Delta v,\Delta w$	disturbances in linear velocities
α	angle of attack of X body axis to relative wind, deg

β	sideslip angle, deg
θ	pitch angle, deg
ϕ	bank angle, deg
ψ	yaw angle, deg
C_{l_β}	rolling-moment coefficient due to sideslip
C_{m_α}	longitudinal static derivative, per deg
C_{m_q}	damping-in-pitch derivative, per radian
C_{n_β}	directional stability derivative, per deg
C_{n_r}	damping-in-yaw derivative, per radian
ω_θ^2	nondimensional pitch frequency squared
ω_ψ^2	nondimensional yaw frequency squared

Subscripts:

o	initial value
max	maximum value
res_θ	refers to resonance in pitch
res_ψ	refers to resonance in yaw

A dot over a symbol indicates differentiation with respect to time.

RESULTS AND DISCUSSION

Several of the fighter-type airplanes presently being flown have exhibited a strong coupling between their lateral and longitudinal modes of motion, particularly in rolling maneuvers. This coupling has led in some instances to very large, essentially uncontrollable airplane motions

in pitch and yaw. Two airplanes currently being flight tested by the National Advisory Committee for Aeronautics and which have experienced violent coupled motions are shown in figure 1. The airplane on the right is an unswept-wing airplane of aspect ratio 3.09 and that on the left is a 45° swept-wing design of aspect ratio 3.56. Both of these airplanes have their mass concentrated primarily in the fuselage, as evidenced by the values of the inertia parameter $\frac{I_Y - I_X}{I_Z}$ shown in the figure for the respective airplanes. This parameter approaches unity for designs which have extremely low inertia in roll relative to the inertia in pitch and yaw. For comparison, for fighters of World War II this parameter was of the order of 0.3 or 0.4.

Results of a recent flight of the unswept-wing airplane are presented in figure 2. The maneuver shown is an abrupt aileron roll from level flight at $M = 1.05$ at an altitude of 30,000 feet. The parameters plotted are sideslip angle, angle of attack, rolling velocity, and the control deflections applied by the pilot. A sideslip angle of 20° was obtained in this maneuver, and, in the 1/2-second time interval between 4.5 seconds and 5.0 seconds, the angle of attack changed from -13° to +19°. This change in α corresponds to a change in normal acceleration from roughly -6g to +7g. Results of a similar flight of the swept-wing airplane are presented in figure 3. The maneuver is an abrupt aileron roll from level flight at $M = 0.70$ at an altitude of 32,000 feet. The maximum sideslip angle encountered was in excess of -25°, and the angle of attack, although not recorded below -16° because of the range of the measuring instrument, was estimated to have been larger than -25°. These large motions impose high loads on both the airplane and pilot, and hence are dangerous as well as undesirable. A point of interest is that the initial variations in α and β are different for the two airplanes discussed although the rolling velocity for both cases is negative. This difference is attributable to the fact that the longitudinal principal axis of inertia is initially above the flight path for the swept-wing airplane whereas for the unswept-wing airplane this axis is initially below the flight path.

The purpose of this paper is to bring to the attention of the autopilot designer the existence of these violent coupled motions, and to discuss the results of some analog studies which indicate that the severity of the pitch-yaw divergences which have been encountered might be alleviated by use of various types of automatic stabilization or regulation. These studies were carried out by NACA personnel at the Langley Aeronautical Laboratory and at the NACA High-Speed Flight Station.

In the theoretical approach to the problem it was necessary to use nonlinear equations of motion to represent the airplane dynamic characteristics. These equations, referred to airplane body axes, are as follows:

$$m\left[\dot{u} + q(w_o + \underline{\Delta w}) - \underline{rv}\right] = F_X + W l_3$$

$$m\left[\dot{v} + r(u_o + \underline{\Delta u}) - p(w_o + \underline{\Delta w})\right] = F_Y + W m_3$$

$$m\left[\dot{w} + \underline{pv} - q(u_o + \underline{\Delta u})\right] = F_Z + W n_3$$

$$I_X \dot{p} - I_{XZ}\dot{r} + \underline{(I_Z - I_Y)qr - I_{XZ}\,pq} = L'$$

$$I_Y \dot{q} - \underline{(I_Z - I_X)pr + I_{XZ}(p^2 - r^2)} + I_{X_e}\omega_e r = M'$$

$$I_Z \dot{r} - I_{XZ}\dot{p} + \underline{(I_Y - I_X)pq + I_{XZ}\,qr} - I_{X_e}\omega_e q = N'$$

$$\dot{l}_3 = m_3 r - n_3 q$$

$$\dot{m}_3 = n_3 p - l_3 r$$

$$\dot{n}_3 = l_3 q - m_3 p$$

These general equations of airplane motion have been modified to include the gyroscopic moments due to the rotating engine. For purposes of comparison the nonlinear terms, which normally are neglected in the analysis of small motions, are underlined. These terms will generally be most important for airplanes which have low inertia in roll relative to that in pitch and yaw, and which are capable of fairly high rolling velocities. Inclusion of these nonlinear coupling terms was necessary in this investigation and the solution of these equations had to be obtained from some computing machine such as an analog computer.

In order to determine if the large motions presented in figure 3 for the swept-wing airplane could have been predicted from these nonlinear equations of airplane motion, this particular flight run was simulated on an analog computer. In this simulation it was assumed that the component of the airplane velocity along its X-axis was constant, which reduced the problem to five degrees of freedom. Estimates of the airplane's mass and aerodynamic characteristics were obtained from available wind-tunnel tests, flight data, and theory. Figure 4 shows the comparisons between the flight record and the analog results. Flight results are shown as dashed lines and the calculated motions as solid curves. The agreement between the flight results and the analog calculations for the time interval shown indicates that the simulation was sufficiently accurate to predict the existence of the large motions encountered in flight. In order to obtain the agreement shown in this

figure, it was necessary to make some adjustments in the preliminary estimates of the airplane stability derivatives. In particular, it was necessary to take into account the variation with angle of attack of the rolling-moment coefficient due to sideslip C_{l_β}. On the basis of this agreement, additional calculations were made for various amounts of aileron deflection for this particular flight condition so as to obtain an indication of the response characteristics of the airplane in aileron-induced rolls. The basic input was a ramp aileron deflection which was held deflected until the airplane rolled to a specific bank angle and the aileron was then returned to zero deflection. The rudder and elevator were assumed to be fixed in these maneuvers. The bank angles for which results were obtained were $\pm 90^\circ$ and $\pm 360^\circ$.

Results typical of those gotten from these calculations for left rolls of 90° and 360° are presented in figure 5. The aileron deflection in each of these cases was such as to give a maximum rolling velocity of -1.5 radians per second. The quantities tabulated in these and similar runs were the maximum rolling velocity, maximum sideslip, and maximum disturbance in angle of attack during the rolling maneuver. For cases in which the values of $\Delta\beta$ and $\Delta\alpha$ obtained when the aileron deflection was reduced to zero, which is the recovery phase of the maneuver, exceeded the values calculated in the maneuver, these values were also tabulated. A summary of the results obtained over the airplane rolling-velocity range is given in figures 6 and 7. Results for left rolls are presented in figure 6 and results for right rolls are presented in figure 7. The maximum changes in sideslip angle and angle of attack are plotted against the maximum rolling velocity obtained in the rolling maneuvers. The difference between the left and right rolls is due to the asymmetric engine gyroscopic moments which were mentioned earlier. The magnitudes of $\Delta\alpha$ and $\Delta\beta$ in the 90° rolls are seen to be fairly small. The worse condition shown appears to be the 360° left roll and the subsequent discussion will be limited to this case. As the aileron deflection, and hence the maximum rolling velocity, is increased, there is a consistent increase in the maximum variations in sideslip angle and angle of attack for rolling velocities up to -2.6 radians per second. The values of approximately 24° for $\Delta\beta$ and 14° for $\Delta\alpha$ were obtained for this roll rate. For purposes of comparison, the values of rolling velocity which produce resonance in pitch and yaw, based on a steady-rolling analysis (see refs. 1 and 2), are shown by the dashed vertical lines. Some preliminary analysis of the steady-rolling case has indicated that variations in certain of the airplane stability derivatives could have an appreciable effect on the magnitudes of α and β encountered in these rolling maneuvers. Figure 8 presents divergence boundaries for the swept-wing airplane. These boundaries, the construction of which is discussed in references 1 and 2, are plotted as a function of the airplane pitch and yaw natural frequencies nondimensionalized to rolling velocity. The solid curve is for the basic airplane. It can be shown that the position in this plane of the pitch and yaw

frequencies of a given airplane, nondimensionalized to rolling velocity, falls on a straight line similar to the one shown in the figure. The slope of this line is determined from the ratio of the square of the pitch and yaw natural frequencies. For $p = 1$ radian per second the values of ω_θ^2 and ω_ψ^2 are equivalent to their dimensional counterparts, and this point is spotted on the straight line in order to show the dimensional values of the pitch and yaw frequencies of the swept-wing airplane. As the rolling velocity increases, the airplane frequency parameters move down this line and for a value of $\omega_\psi^2 = 0.70$ cross the divergence boundary. For the swept-wing airplane, this crossing of the boundary occurs for a rolling velocity of 1.7 radians per second. The boundary is again crossed for $\omega_\theta^2 \approx 1$ which corresponds to a rolling velocity of 2.2 radians per second. For values of rolling velocity between 1.7 and 2.2 radians per second, this simplified analysis predicts a divergence, and it is these values which were indicated by the vertical lines in figure 6.

It is apparent from figure 8 that this divergent condition can be eliminated in at least two ways. Variations in the airplane dimensional pitch or yaw frequencies can rotate this line to prevent its passing through the unstable region, or the boundaries can be moved with respect to the line which represents the swept-wing airplane to effect a similar result. These boundaries can be shifted by increasing the damping in pitch or yaw as indicated by the dashed boundaries for increased damping.

For the condition shown, this line can be rotated into the stable region by increasing the yaw natural frequency through increases in C_{n_β} or decreasing the pitch natural frequency through a decrease in C_{m_α}. However, for too large a variation in these parameters, the line will be rotated to a position for which it will pass through the lower branch of the divergence boundaries. It appears that a good rule of thumb would be to rotate the line to a position where the airplane pitch and yaw frequencies are approximately equal.

Results will be presented in the subsequent figures which indicate the effect of variations in the static derivatives C_{n_β} and C_{m_α} and in the damping derivatives C_{n_r} and C_{m_q}. Cases will be discussed for increases in C_{n_β} which rotate the line clockwise from its basic orientation to the stable region and then to a position for which it passes through the pitch divergence boundary for a rolling velocity approximately equal to the pitch natural frequency. For C_{m_α}, a variation will be discussed which rotates this frequency locus from its basic position to a position in the stable region of this plot. Cases will be discussed for C_{n_r} and C_{m_q} which shift the boundaries in the direction indicated by the dashed lines (see fig. 8), and hence put the basic

frequency locus in a stable region. In the subsequent figures, values of rolling velocity are plotted which correspond to the resonant values predicted by the simplified steady-rolling analysis.

The effect of varying the directional stability parameter C_{n_β} is presented in figure 9. This derivative could be varied artificially by deflecting the rudder proportional to sideslip angle. The curve for $C_{n_\beta} = 0.001$ corresponds to the airplane without automatic controls. As C_{n_β} is increased to 0.002, the maximum variations in sideslip and angle of attack computed for these rolling maneuvers are markedly reduced. It appears, however, that an increase to 0.004 results in a condition during recovery which is about as bad as that which exists for $C_{n_\beta} = 0.001$. For this value of C_{n_β}, the frequency locus has been rotated to a position such that it passes through the lower boundary for a rolling velocity approximately equal to the pitch frequency, and there is seen to be a large positive peak in $\Delta\alpha$ which exceeds the negative values calculated for the maneuver. It is apparent from figure 9, however, that the large variations in angle of attack and sideslip experienced by this airplane in rolling maneuvers are largely due to a basic deficiency in directional stability and, if the existing value of C_{n_β} of 0.001 could be increased to a somewhat higher level by artificial means or by redesign of the vertical tail, the airplane characteristics would be improved.

Results are presented in figure 10 for variations in the longitudinal static derivative C_{m_α}. The curve for $C_{m_\alpha} = -0.006$ corresponds to the basic airplane. As C_{m_α} is reduced to -0.003, for which case the frequency locus is in the stable region for all values of p, the α- and β-motions are seen to be substantially reduced.

Results are shown in figure 11 to show the effect of the damping-in-yaw derivative C_{n_r}. This derivative could be varied by use of a "yaw damper," in which the rudder is deflected proportional to yawing velocity. The value of C_{n_r} estimated for the swept-wing airplane for the flight condition being discussed is -0.10. On the basis of the estimated effectiveness of the airplane rudder, it appears that an increase in C_{n_r} to -1.0 is approximately of the order of magnitude which could be realized from a yaw damper for this flight condition. As C_{n_r} is assumed to be varied from its basic value of -0.10 to -1.0, there is seen to be an improvement in the airplane characteristics in these aileron-induced rolls, although the improvement is less than that calculated for C_{n_β} and C_{m_α}.

Results are presented in figure 12 for variations in the damping-in-pitch derivative C_{m_q}. This derivative could be varied by a pitch damper which deflects the stabilizer proportional to pitching velocity. As C_{m_q} is assumed to be varied from its basic value of -3.5 to -35.0, the maximum value of $\Delta\beta$ is reduced from 24° to 6° and the angle-of-attack variation is reduced from 14° to 6°. This value of C_{m_q} is approximately in the range which could be realized from a pitch damper for this particular airplane and flight condition.

CONCLUDING REMARKS

It should be emphasized that these preliminary calculations were made for only one flight condition and for one type of maneuver, and therefore no attempt should be made to generalize the results presented to other conditions of altitude and Mach number and to other maneuvers. However, the trends indicated by these results are believed to be qualitatively representative of those which would be obtained through use of the automatic controls discussed.

The primary conclusions which can be drawn from this paper do, however indicate that (1) certain of the fighter-type airplanes which are being flown today are highly susceptible to divergences in angle of attack and sideslip during rolling maneuvers and (2) people in the automatic control field may be in a position to assist in the solution of this problem by equipping airplanes with autopilots which will reduce the severity of these undesirable motions.

Langley Aeronautical Laboratory,
National Advisory Committee for Aeronautics,
Langley Field, Va., May 11, 1955.

REFERENCES

1. Phillips, William H.: Effect of Steady Rolling on Longitudinal and Directional Stability. NACA TN 1627, 1948.

2. White, R. J., Uddenberg, R. C., Murray, D., and Graham, F. D.: The Dynamic Stability and Control Equations of a Pivoted-Wing Supersonic Pilotless Aircraft, With Downwash, Wake and Interference Effects Included. Doc. No. D-8510, Boeing Aircraft Co., Jan. 9, 1948.

CHARACTERISTICS OF AIRPLANES

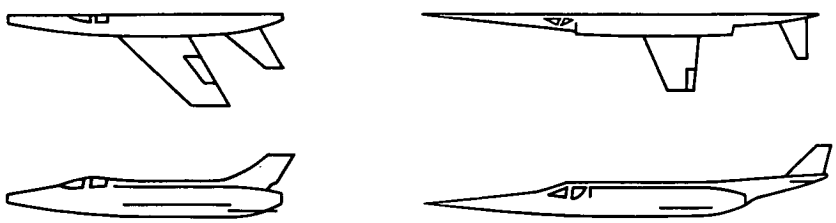

$\Lambda_{\frac{c}{4}} = 45°$

$A = 3.56$

$\frac{I_Y - I_X}{I_Z} = 0.72$

$\Lambda_{\frac{3}{4}c} = 0°$

$A = 3.09$

$\frac{I_Y - I_X}{I_Z} = 0.89$

Figure 1

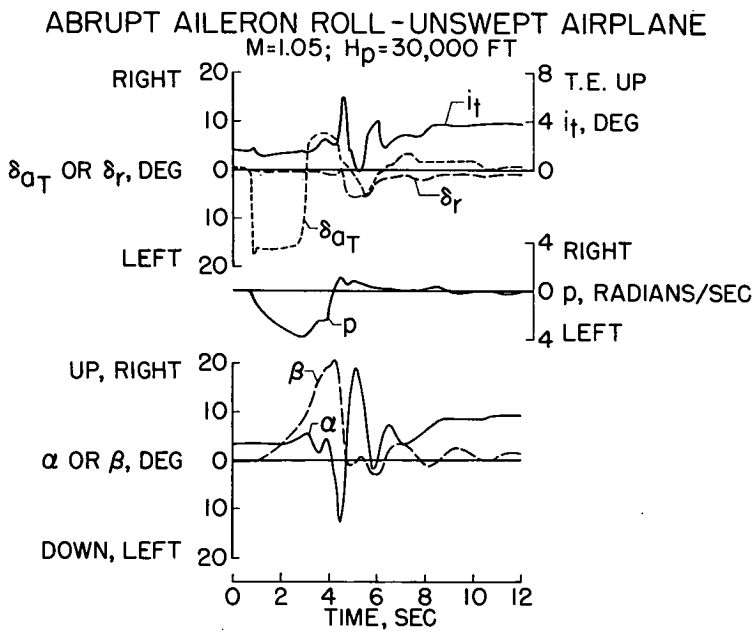

Figure 2

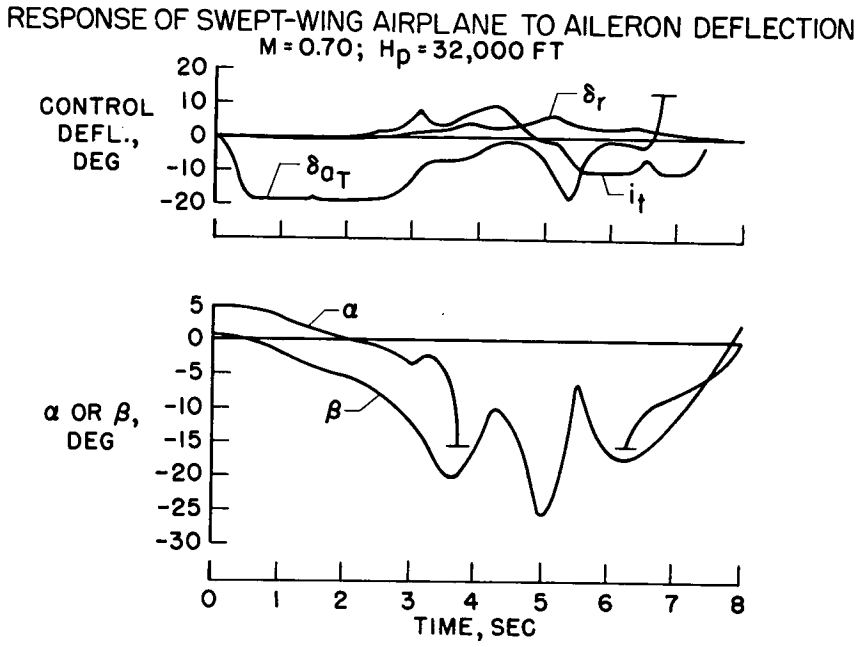

Figure 3

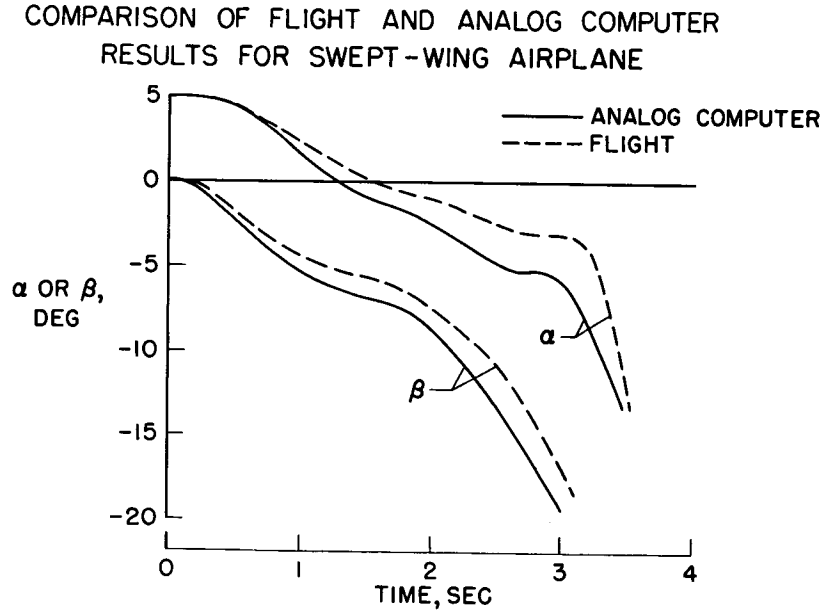

Figure 4

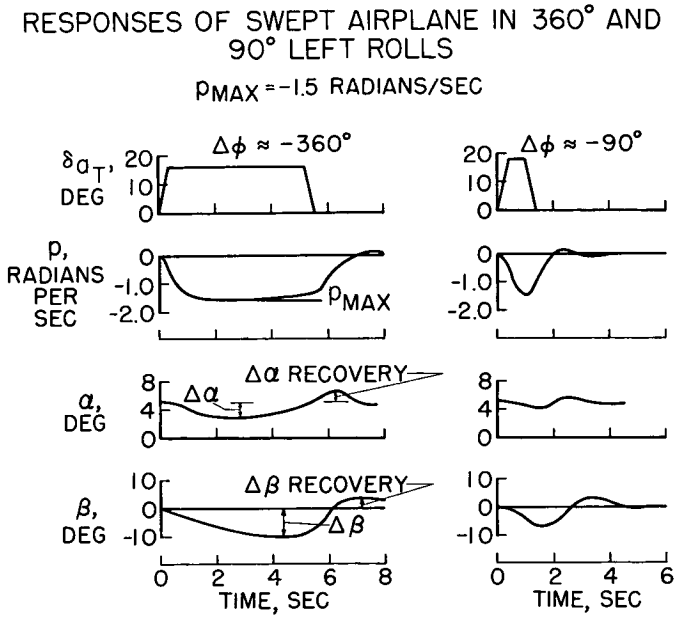

Figure 5

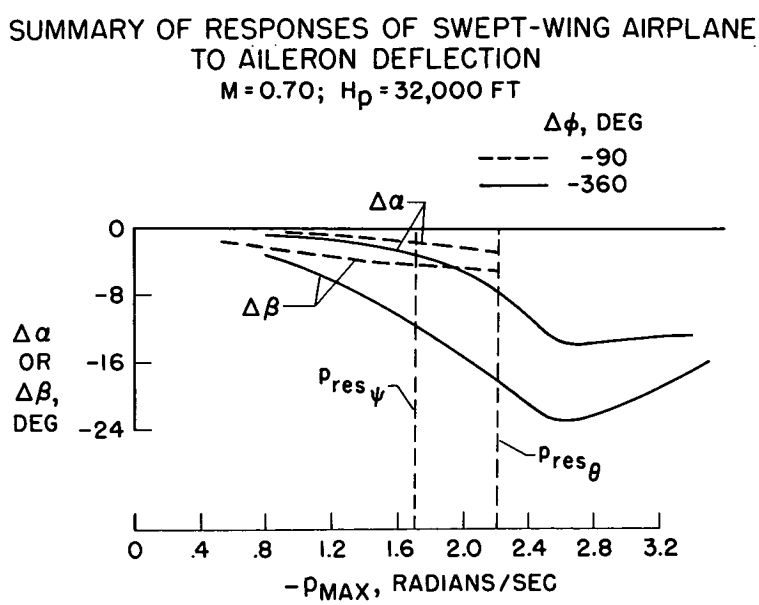

Figure 6

SUMMARY OF RESPONSES OF SWEPT-WING AIRPLANE TO AILERON DEFLECTION

M = 0.70; H_p = 32,000 FT

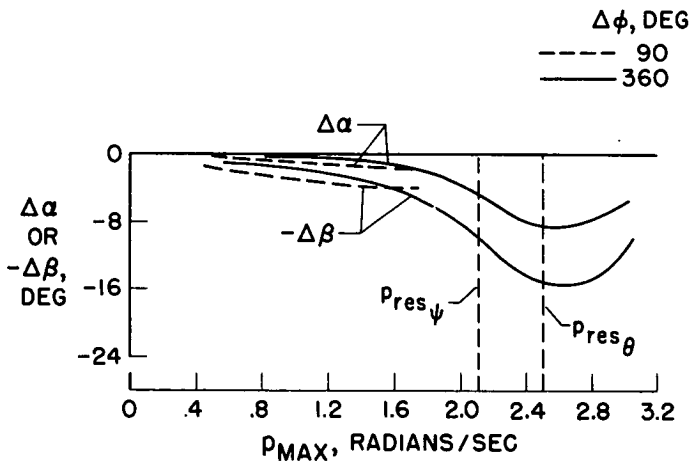

Figure 7

DIVERGENCE BOUNDARIES – STEADY ROLLING

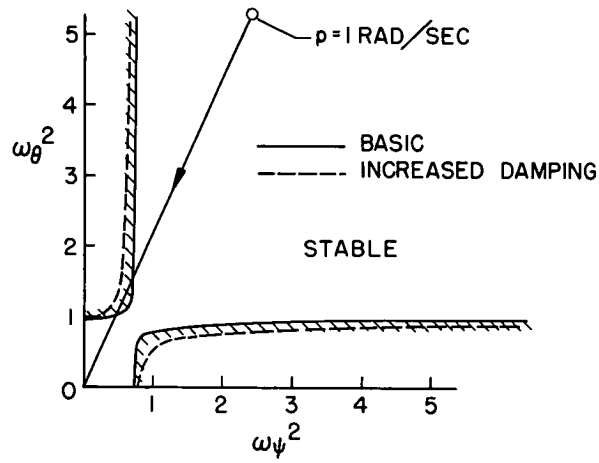

$$\omega_\theta^2 = \frac{-C_{m_\alpha} qS\bar{c}}{I_Y p^2} \qquad \omega_\psi^2 = \frac{C_{n_\beta} qSb}{I_Z p^2}$$

Figure 8

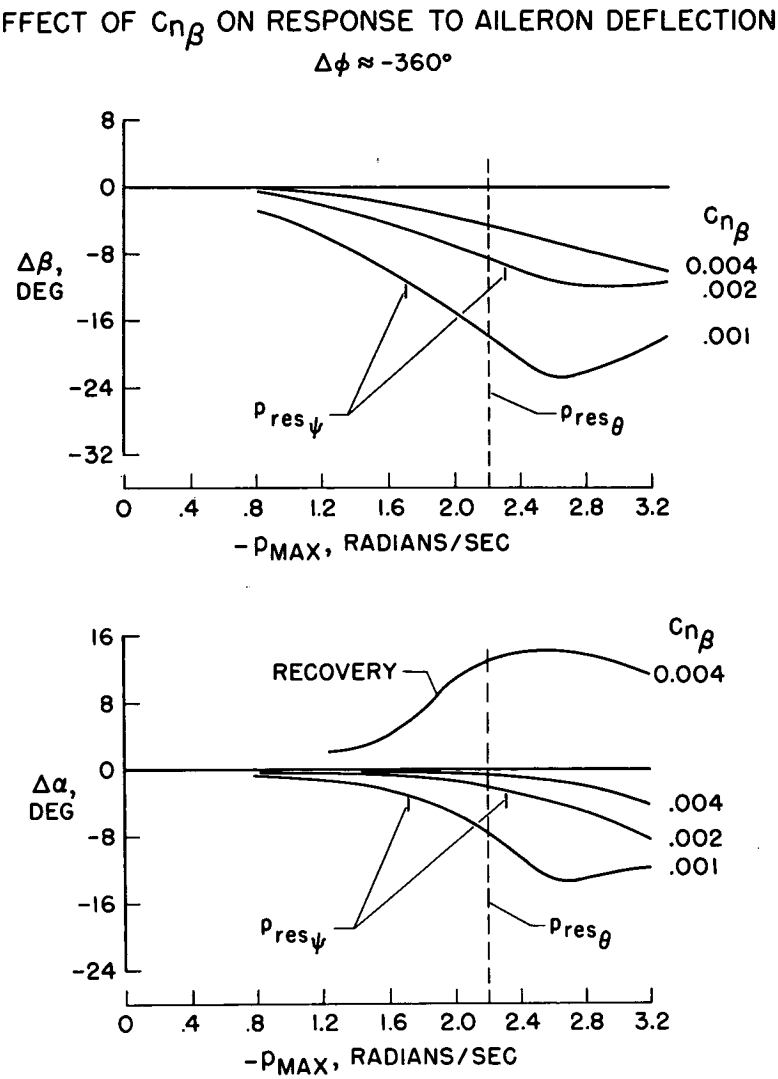
EFFECT OF C_{n_β} ON RESPONSE TO AILERON DEFLECTION
$\Delta\phi \approx -360°$
8
0
-8
-16
-24
-32
$\Delta\beta$, DEG
C_{n_β}
0.004
.002
.001
p_{res_ψ}
p_{res_θ}
0 .4 .8 1.2 1.6 2.0 2.4 2.8 3.2
$-p_{MAX}$, RADIANS/SEC
16
8
0
-8
-16
-24
$\Delta\alpha$, DEG
RECOVERY
C_{n_β}
0.004
.004
.002
.001
p_{res_ψ}
p_{res_θ}
0 .4 .8 1.2 1.6 2.0 2.4 2.8 3.2
$-p_{MAX}$, RADIANS/SEC

Figure 9

EFFECT OF C_{m_α} ON RESPONSE TO AILERON DEFLECTION

$\Delta\phi \approx -360°$

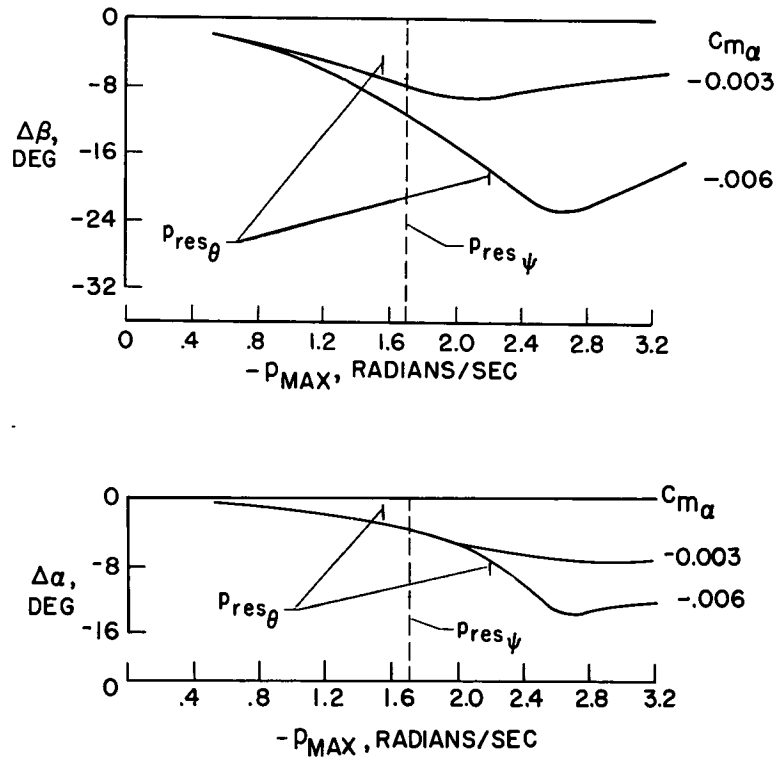

Figure 10

EFFECT OF C_{n_r} ON RESPONSE TO AILERON DEFLECTION

$\Delta\phi \approx -360°$

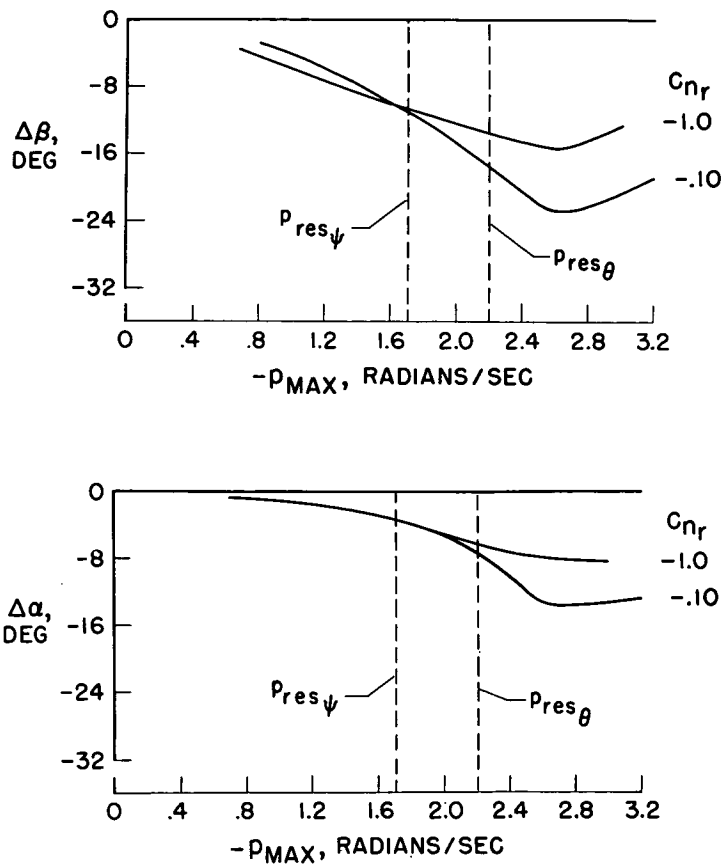

Figure 11

EFFECT OF C_{m_q} ON RESPONSE TO AILERON DEFLECTION

$\Delta\phi \approx -360°$

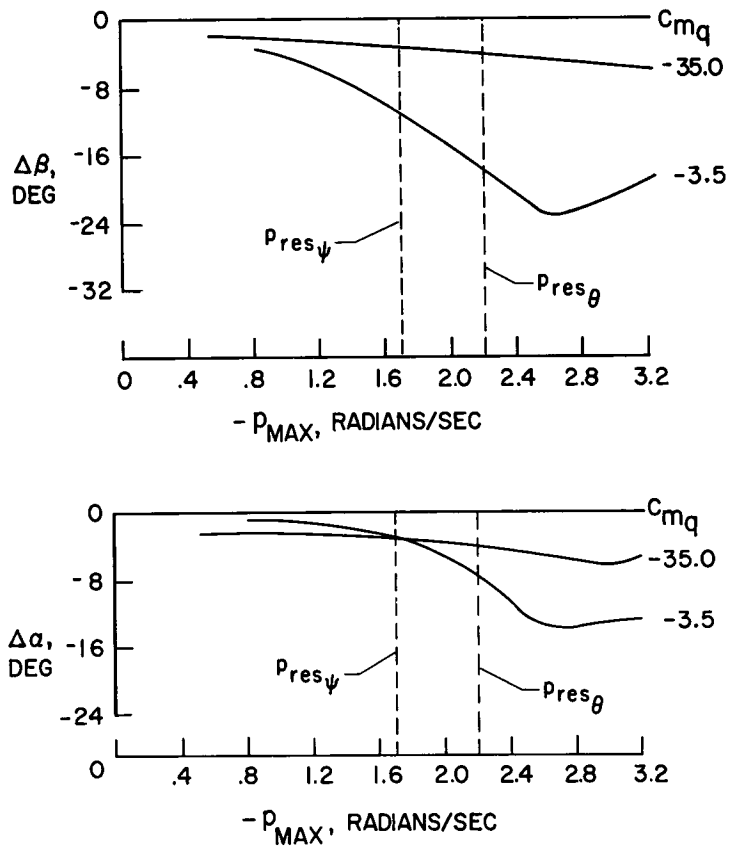

Figure 12